Response of lightly overconsolidated clay under irregular cyclic loading and comparison with predictions from the strain accumulation procedure

KRISTOFFER S. SKAU*, BIRGITTE MIDSUND DAHL*, HANS PETTER JOSTAD*, YUSUKE SUZUKI*, JEROME DE SORDI† and OLE HAVMØLLER†

Offshore wind turbine foundations are designed to withstand environmental loads from the wind and waves, both of which are cyclic in nature. The current design methods consider site-specific cyclic load histories and typically require these to be translated from a time–load history with irregular characteristics to an idealised history of parcels of cycles with uniform amplitude and constant average load. The Rainflow counting method is typically used for this translation. The idealised history is then applied in a design method, for example the strain accumulation method. These methods assume that the idealised load history will give approximately the same effect on the soil as the irregular time history. This paper investigates this assumption by a laboratory test programme where the soil response under realistic irregular loading is compared with the response under idealised loading. The laboratory programme consists of cyclic direct simple shear tests on lightly overconsolidated North Sea clay. For most problems, the test results suggest that the assumption is reasonable and represents a convenient simplification for practical design. However, for load histories with large average load, prediction of permanent strain based on idealised histories may underestimate the strain observed in tests with irregular time histories.

KEYWORDS: coastal, marine and offshore geotechnics; design methods & aids; laboratory characterisation and sampling of soils; laboratory tests; offshore foundations; offshore renewable energy; wave loading

INTRODUCTION

Offshore foundations supporting wind turbines are designed to withstand environmental loads with cyclic nature from the wind and waves. During extreme storm events, the foundation may be subjected to thousands of cycles, and reliable methods to predict cyclic strain and cyclic stiffness are critical for an optimal and reliable foundation design. Cyclic loading may significantly affect the behaviour of soil and foundations, and thus the subject has been an important part of geotechnical research since early studies in the late 1960s – for example, Seed & Lee (1966), Seed (1968), Ishihara *et al*. (1975) and Andersen (1976).

A significant part of this research has focused on developing models and methods for the design of offshore foundations. Many of these models describe the response on an incremental stress–strain basis. Such models are sometimes referred to as implicit (or intrinsic) models. The models proposed by Mróz *et al*. (1981), Taiebat & Dafalias (2008) and Liu *et al*. (2019) are examples of such implicit models. Another category of models has been developed to capture the effect of a very large number of cycles. These models have typically been referred to as explicit (or extrinsic) models. The models describe the response not by considering a stress increment but through a cyclic history where the response is computed by an explicit function of number of cycles, cyclic stress amplitude and average stress. The high cyclic accumulation model for sand described in the papers by Niemunis *et al*. (2005) and Wichtmann *et al*. (2009), and the numerical procedure for monopiles proposed by Achmus *et al*. (2009), are examples of such explicit models. For a large number of cycles, the explicit models are efficient and generally considered to be more accurate than implicit (or intrinsic) models.

To apply the explicit models, it is necessary to translate the irregular time history to an idealised history with groups of cycles with similar load amplitudes and a representative average load and load frequency. Rainflow counting (Matsuishi & Endo, 1968) is typically used to translate the irregular time history to the idealised representation. The idealised history is then evaluated by a design method that includes the soil's resistance to cyclic loading. Most methods used in design practice are based upon the same idealised description of the load history – for example, the Norwegian Geotechnical Institute (NGI) procedure explained in the papers by Andersen (2015) and Skau & Jostad (2014), the models proposed by Achmus *et al*. (2009) and Leblanc *et al*. (2009) specifically for monopiles, and the models based on experimental testing on sand by Wichtmann (2005). All the methods rely on the assumption that an irregular time history and the equivalent idealised history will have the same effect on the soil stiffness and strength. However, the literature lacks experimental evidence to support the assumption.

Andersen *et al*. (1992) studied the effect of the order of the cyclic groups by an experimental laboratory programme on normal and overconsolidated clay. The study showed that the order of the groups influenced the final strain level. However, the influence was moderate and conservative in design if the history was organised with the amplitudes of the groups in ascending order. This approach has been adapted in practical design and considered to be sufficiently accurate. The challenges related to the translation of irregular load histories were considered by Norén-Cosgriff *et al*. (2015); they showed that the method used for load history translation could affect the degradation predicted by the accumulation procedure (Andersen, 2015). The paper considered translation by the

Manuscript received 31 May 2021; revised manuscript accepted 14 January 2022.
Discussion on this paper is welcomed by the editor.

*NGI, Oslo, Norway.
†Equinor, Stavanger, Norway.

Rainflow counting procedure and a new procedure introduced in the paper. Based on the observed difference between the two methods of translation, the paper recommends that laboratory testing using true time histories should be performed to evolve the empirical basis for comparison of different translation methods.

Zografou *et al.* (2019) recently published results from a laboratory test programme on normally consolidated kaolin clay focusing on the organisation of histories after the translation to idealised histories has been performed. The study specifically focused on how the total strain depends on the order of groups of cyclic loads in idealised histories. The results give experimental evidence for the assumption in current design practice where the groups of cyclic loads are organised based on ascending amplitude. The study concludes in agreement with Andersen *et al.* (1992), who also observe the total strain to be larger at the end of history when the group of cycles with the largest amplitude is applied at the end of the history.

These studies provide experimental evidence of the reliability of design methods and how load representation affects soil behaviour. The study documented in this paper applies physical testing for considering the effect of load history representation and focuses on the translation of load histories from how they originally occur, as irregular time histories, to idealised histories required in most design methods.

Physical testing on lightly overconsolidated clay complements the theoretical study in the work of Norén-Cosgriff *et al.* (2015). The focus on translation of irregular time histories complements earlier studies by examining the assumption in the design step before any re-ordering of cyclic groups addressed in the papers by Andersen *et al.* (1992) and Zografou *et al.* (2019). It is vital to understand the translation from irregular time histories to idealised histories since the assumption is used in most design methods.

In this paper the term 'irregular loading' is used in a different way compared to existing papers. In the papers by Andersen *et al.* (1992) and Zografou *et al.* (2019), each group with constant cyclic amplitude is fixed but re-arranged according to each other. In this paper, irregular loading refers to load histories that are truly irregular time histories as they appear in nature from wind and waves. The authors are not aware of any experimental study that compares the cyclic degradation caused by a truly irregular time history with the cyclic degradation caused by its idealised representation.

The paper presents the results from the cyclic test programme of direct simple shear (DSS) tests (Bjerrum & Landva, 1966) of overconsolidated clay. The results from these tests have been used further to: (*a*) evaluate the assumption of translation of irregular load histories to idealised load histories; (*b*) evaluate the reliability of the accumulation procedure including the counting methodology; and (*c*) give recommendations to design practice based on the findings in the study.

THE NGI PROCEDURE ACCOUNTING FOR CYCLIC LOADING

This study evaluates the laboratory results in the framework of the NGI procedure for cyclic loading. The procedure is based on cyclic laboratory element testing along relevant stress paths. The applied stress and resulting strain and pore pressure are divided into cyclic and average parts as illustrated in Fig. 1. After several tests with different shear stress levels and cyclic-to-average shear stress ratios, the results are interpreted and presented in contour diagrams as described by Andersen (2015). The diagrams then contain information about the relationship between cyclic shear stress (τ_{cy}), average shear stress (τ_a), cyclic shear strain (γ_{cy}), average

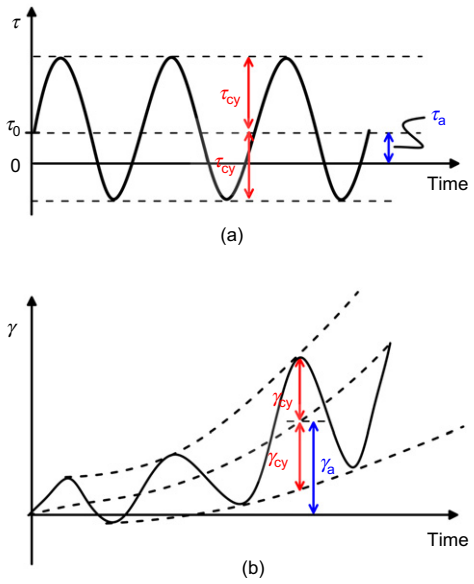

Fig. 1. Definition of cyclic and average: (a) shear stress; (b) strain (after Andersen, 2015)

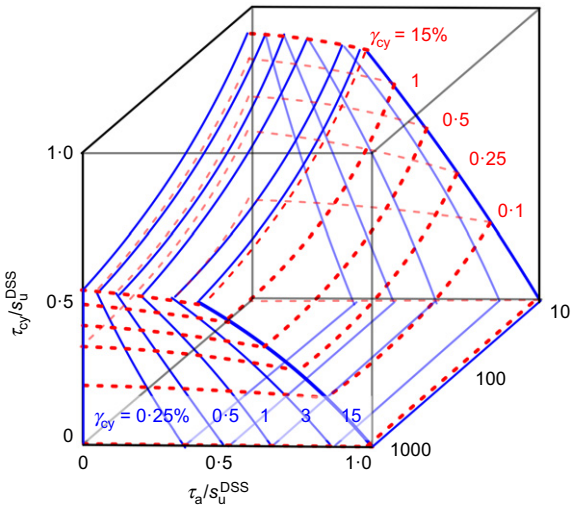

Fig. 2. Direct simple shear (DSS) contour diagram with cyclic (τ_{cy}) and average shear strain (τ_a) in a 3D space of cyclic shear stress (τ_{cy}). Average shear stress (τ_a) and number of cycles N (after Andersen, 2015)

shear strain (γ_a), average pore pressure (u_a) and number of applied cycles (N). The diagrams are based on triaxial compression tests, triaxial extension tests (Lade, 2016) and DSS tests (Bjerrum & Landva, 1966). Fig. 2 shows an example of a full three-dimensional (3D) DSS contour diagram where the cyclic and average shear strain (γ_{cy} and γ_a) are given as functions of cyclic and average shear stress (τ_{cy} and τ_a) and number of cycles (N). The contour diagrams can then be used to account for the effect of a cyclic shear stress history, which must first be idealised into groups with shear stress cycles of similar amplitude and average shear stress. Please note that a cross-section of the diagram in Fig. 2 can be extracted and plotted as a 3D diagram. Fig. 4 later in the paper is an example of such a two-dimensional (2D) cross-section of the diagram. The history can then be applied to or followed in contour diagrams according to the accumulation procedure proposed by Andersen (2015), and the number of equivalent cycles, N_{eq}, can be determined. The physical meaning of N_{eq} is that a full irregular shear stress

history can be represented by a number of consecutive equivalent cycles (N_{eq}) of a constant cyclic and average shear stress. In practice, the accumulation procedure is normally performed in a 2D cross-section of a contour diagram. Examples of strain accumulation are shown later in the paper. The accumulation procedure explained herein was used to predict the final strain in all the laboratory tests presented in this paper.

LABORATORY PROGRAMME AND TEST APPROACH

Test material

The test material is clay from the Utsira High area in the North Sea, sampled between 10 and 25 m below the seabed. The clay is 'lightly' overconsolidated as the result of glacial compaction. Based on the current geological model and laboratory test results, the depositional context of the clay seems to correspond to a transitional period between a glacial maximum (approximately 22–27 000 years ago) and the start of a deglaciation period when the area was very close to sea level. The clay has a water content, $w =\sim 21\%$, plasticity index, $I_p =\sim 18\%$, liquid limit, $w_L =\sim 35\%$, fines content around 75% and medium to high undrained shear strength (undrained shear strength in triaxial compression, s_{uC} between 50 and 165 kPa). All samples considered in this paper are taken from the same borehole. Soil material was collected using a 3 in. (7·62 cm) thin-walled hydraulic piston lowered inside a borehole drilled with a heave-compensated rotary system, a seabed guide base and American Petroleum Institute (API) drill pipes. The specific samples tested in the laboratory programme reported herein had an overconsolidation ratio (OCR) value of 2·6 (interpreted based on oedometer results not included in this paper) and a strength-to-vertical stress ratio $(s_u^{DSS}/\sigma'_{v0}) = 0{\cdot}70$ with in situ effective stress conditions, σ'_{v0}, calculated based on an average effective soil unit weight, $\gamma' = 10{\cdot}3$ kN/m^3.

Test equipment and procedures

The laboratory test programme includes both monotonic and cyclic constant-volume DSS testing. The DSS tests were conducted in an electro-mechanical dynamic DSS device manufactured by GDS Instruments Ltd. Fig. 3 shows a principle sketch of the DSS device. The device consists of two electro-mechanical actuators, one for vertical loading and one for horizontal loading. The actuators are capable of measuring forces up to 5 kN with operating frequency of 5 Hz. The top cap and base pedestal have been modified by the NGI laboratory such that a reinforced-wire membrane can be used for the lateral confinement of the specimen. Two drainage tubes in the top cap and two in the base pedestal allow for flushing of the system and the specimen, consolidation of the specimen and indication of volume change during constant-volume shearing. The device is equipped with a height control system to keep the specimen height constant during either monotonic or cyclic shearing. This keeps the volume of the specimen constant and simulates undrained conditions.

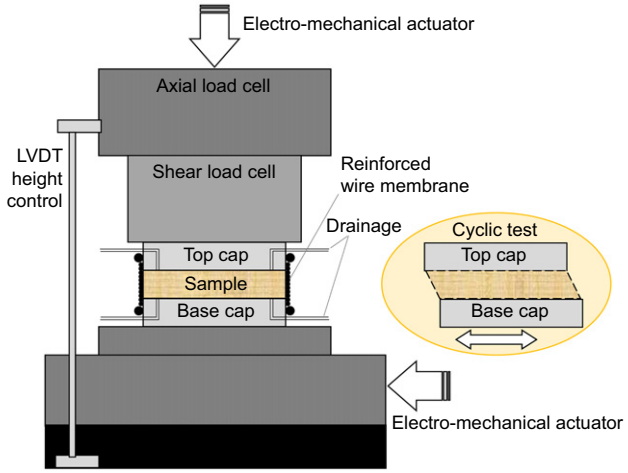

Fig. 3. DSS test set-up (LVDT, linear variable differential transducer)

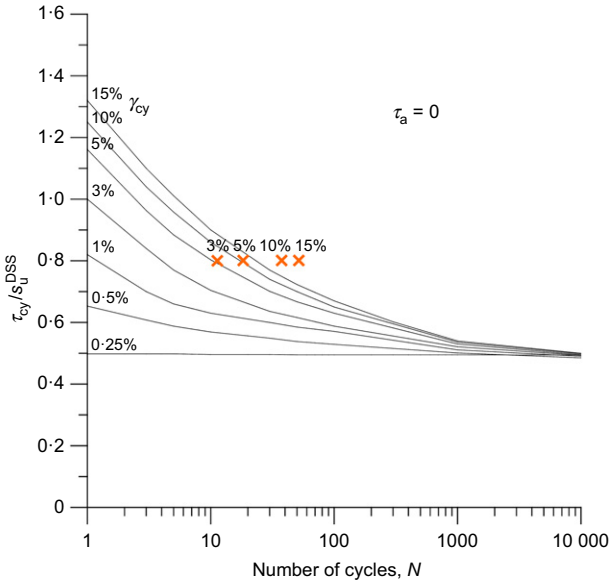

Fig. 4. Contour diagram for ($\tau_a/s_u^{DSS} = 0$) representing cyclic response at a loading frequency of 0·25 Hz. The crosses indicate the test results from 11-B

A test specimen was prepared from the waxed sample by using a cutting ring, a wire saw and a knife to the test the specimen geometry of 16 mm × 66·7 mm (height × diameter). After sample preparation, all specimens were consolidated to 80% of the pre-consolidation vertical stress and then unloaded to the in situ vertical stress level (σ'_{v0}). The in situ stress conditions were calculated based on an average effective soil unit weight, $\gamma' = 10{\cdot}3$ kN/m^3. For the monotonic loading, constant-volume DSS tests were conducted with displacement control at about 80 min/mm – that is, a shear strain rate of about 4·5%/h. The idealised cyclic load history was applied using load-controlled sinuous wave function with predefined average and cyclic stresses. For the irregular cyclic loading histories, a user-defined wave function was used to import loading histories into the software. The load frequencies in the cyclic tests are elaborated later in the paper.

Laboratory test programme

The laboratory programme consisted of two parts. The tests in part 1 were standard monotonic and cyclic tests. These tests served as a basis for defining a contour diagram that was used to determine the stress levels to be applied in the tests with irregular load in part 2. In addition, the contour diagram was used to assess the reliability of the accumulation procedure. Table 1 summarises the tests in part 1. Note that all but two of these tests were performed independently and approximately 1 year prior to the test programme on irregular cyclic loading. The purpose of the two tests, which were executed approximately at the same time as the irregular testing, was to evaluate

Table 1. Summary of tests in part 1 used as basis for establishing the contour diagram for interpretation of the irregular cyclic testing in part 2

	Identifier	Sample depth: m	Monotonic testing		Cyclic testing		
			s_u^{DSS}: kPa	s_u^{DSS}/σ'_{v0}	τ_a/s_u^{DSS}	τ_{cy}/s_u^{DSS}	N
Monotonic tests	14-B-2	13·40	71·7	0·53			
	11-C*	15·85	113·5	0·70			
	12-D-1	17·17	113·7	0·65			
	20-C-1	18·92	153·0	0·80			
Cyclic tests	11-B†	15·68			0	0·80	54·0
	12-D-2	17·21			0·4	0·71	111·8
	12-D-3	17·25			0	0·55	681·5
	12-D-4	17·29			0·4	0·89	5·8
	20-C-2	18·96			0	0·79	24·2
	20-C-3	19·00			0	1·10	1·8
	20-C-4	19·04			0	0·68	27·4

*Performed 1 year later than the others to assess possible effect of storage.
†Performed 1 year later than the others and at a higher rate to adjust the contour diagram to relevant test frequency.

whether the material had changed with time (storage effects) and to adjust the contour diagram to the test frequency relevant for the irregular test programme in part 2. The load frequency in the standard cyclic tests in part 1 was 0·1 Hz, while 0·25 Hz was relevant for part 2. The background for choosing this load frequency will be explained later in the paper. A scaling factor of 1·11 (11% increase) was applied to the cyclic shear stress in the contour diagram to account for the increased frequency (i.e. rate effects). This is consistent with the rate effect given in the paper by Andersen (2015). Fig. 4 shows the contour diagram established in part 1 for the assessment of the irregular tests programme in part 2. The figure shows that the cyclic test 11-B does not show equally good agreement with the contour diagram for all strain levels. However, scaling of the cyclic shear stress (vertical axis) is a convenient method for adjusting contour diagrams to different loading frequencies (Andersen, 2015), and it was chosen not to modify the contours beyond scaling of cyclic shear stress since the original contour diagram was based on several cyclic tests at standard loading frequency and existing contour diagrams from NGI's in-house database. Table 1 also shows a variation in the normalised shear strength from 0·53 to 0·8. In addition to these tests, index testing and cone penetration testing (CPT) were performed at the site and formed the basis for the determination of the best estimate shear strength profile, which was defined to be $(s_u^{DSS}/\sigma'_{v0}) = 0{\cdot}70$ for the depth of the samples used in this study. There is no reason to disregard any of the test results and the variations in shear strength are caused by inherited variations in the naturally deposited material. Research on such materials adds uncertainty to the results compared to synthetic clays consolidated in laboratories (e.g. Zografou *et al.*, 2019). These principal differences in research methodology must be considered when comparing results from different studies.

Part 2 comprises the tests investigating the effect of irregular cyclic loading. The tests were organised by defining test pairs such that one test pair includes an irregular time history and its corresponding idealised history. To evaluate the effect of the two different histories in each test pair, three reference cycles were added at the end of the histories. These reference cycles had the same stress level within a test pair and were equal to the maximum stress cycle in the history. The effect of the irregular history as opposed to the idealised history could then be compared by the similarity of these cycles. Fig. 5 illustrates such a test pair. Other ways of comparison were also discussed prior to the tests as there are no standardised ways of comparing the effect of a cyclic history. One alternative was to reduce the stress cycles to minimise their influence on the response. However, that would have brought the soil closer to a linear behaviour and reduced the differences that the study wanted to identify. Monotonic post-cyclic stress was also considered but rejected since bringing the sample to failure most likely would have wiped out (or hidden) the effect of the earlier history dominated by much smaller strains. The approach with reference cycles was therefore chosen as the best solution for the objective of the study. This method of evaluation is different compared to that of Zografou *et al.* (2019), which had an objective different from the present paper. Zografou *et al.* (2019) compared the strain at the end of the history without any reference cycles and, since the cyclic strain in the last cycle is a function of the cyclic stress applied in that specific stress cycle, it is difficult to isolate the effect of the history upfront, which is the main objective in the present study. This makes direct comparison of the results difficult.

Load histories

All load histories applied in part 2 of the test programme were based on two different irregular load histories. Both are relevant for an ultimate limit state (ULS) load situation and represent the moment load at the mudline. The moment load was extracted from two different global time domain analyses of an offshore wind turbine and includes wind, waves and rotor dynamics.

Load history 1 (Fig. 6(a)) is based on analyses of a 10 MW wind turbine under idling condition and wind speed and sea state conditions with a 50 year recurrence period. The wind turbine foundation is a 9 m dia. monopile and the water depth is 30 m. The selected period represents a 3 h peak period within a 36 h design storm with a wind speed of 38·5 m/s, significant wave height (H_S) of 9·5 m and a spectral peak period (T_p) of 12·3. The situation reflects design load case (DLC) 6·1 but does not include any yaw misalignment (IEC 61400-3; IEC, 2009).

Load history 2 (Fig. 6(b)) is based on analyses of a 6 MW wind turbine under idling condition and wind speed and sea state conditions with a 50 year recurrence period. This is combined with a loss of the electrical network connection causing a yaw error increasing the thrust load. The wind turbine foundation is a 6 m dia. monopile and the water depth is 23·5 m. The selected period represents a 3 h peak period within a 36 h design storm with a wind speed of 42·0 m/s, H_S of 6·9 m and T_p of 12·5 s. The situation corresponds to DLC 6·2 (IEC 61400-3 (IEC, 2009)). This load history has a significant average load throughout the 3 h. This is different to load history 1, which has almost no average load.

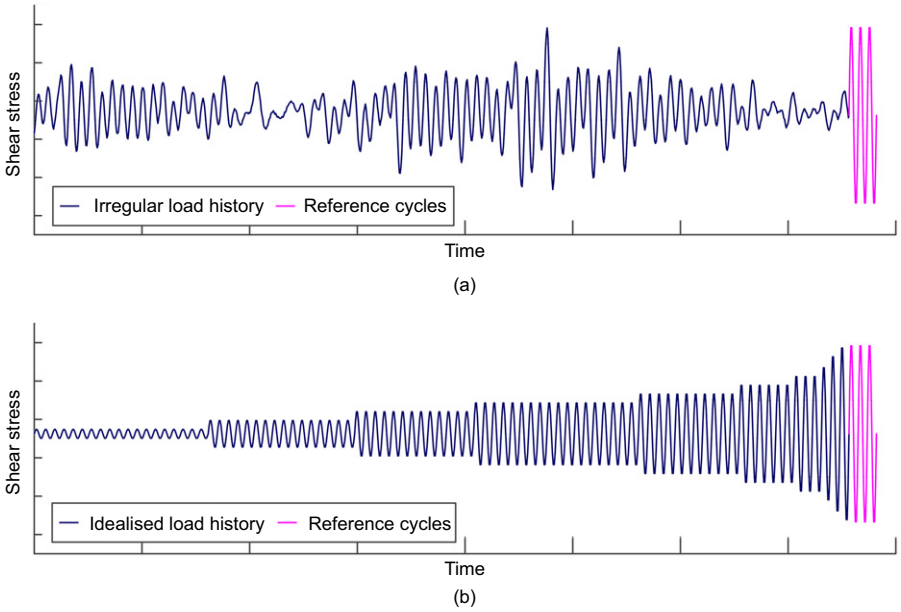

Fig. 5. Illustration of a typical test pair of two representations: (a) an irregular time history; (b) a re-organised history. Both followed by reference cycles for evaluation

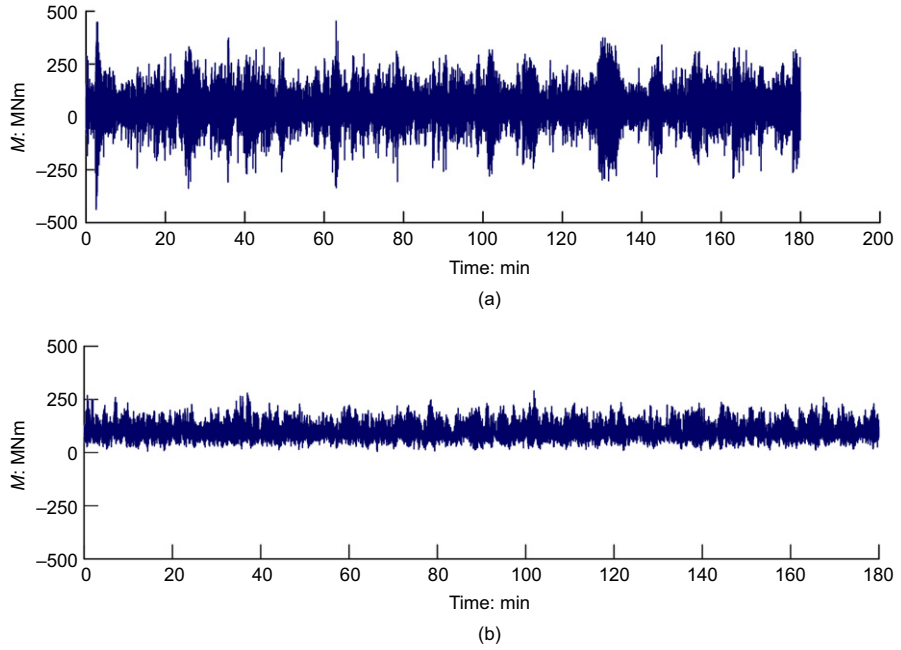

Fig. 6. (a) Load history 1 (negligible average); (b) load history 2 (significant average)

Since the irregular histories contain load cycles with different frequencies, it was necessary to define a representative frequency that was to be applied in the testing programme with idealised load histories. The representative frequency was identified by the peak values in the power spectral densities (PSDs) shown in Fig. 7. Based on Fig. 7, 0·25 Hz was identified as the most representative frequency for both histories. The contour diagram established in part 1 was also scaled to reflect the same load frequency.

Laboratory tests programme – part 2

The moment load at the mudline was scaled to the appropriate shear stress level assuming proportionality between loads and shear stresses in the soil. Since soil elements around a monopile experience different levels of mobilisation, it was reasonable to perform the testing at different mobilisation levels. If the applied shear stress was too small, it would have been difficult to detect differences in strain within a test pair. If the applied shear stress was too large, it would have led to failure, hence comparing strain values would have been of little value. Therefore, stress levels were determined by predicting the strain at the end of test by the accumulation procedure and using trial and error until the preferred strain level was obtained. Fig. 8 shows the trajectory of the accumulation procedure for load history 1, which was scaled to reach a final strain level $\gamma_{cy} = 3\%$. The procedure predicts that to reach this cyclic strain, the history should be scaled such that the maximum stress amplitude is $(\tau_{cy}/s_u^{DSS}) = 0{\cdot}88$. Table 2 summarises all tests and their respective maximum cyclic shear stress and the average shear stress of the full history (average of all time stamps). The

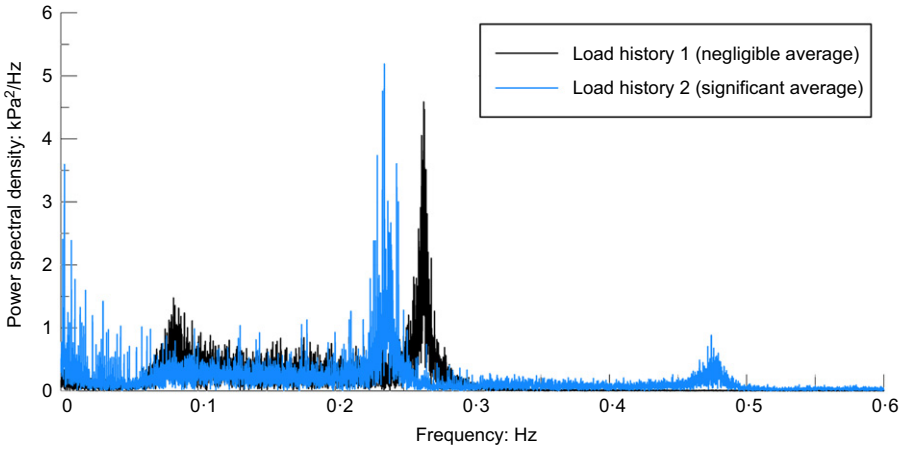

Fig. 7. Power spectral density (PSD) for the load histories

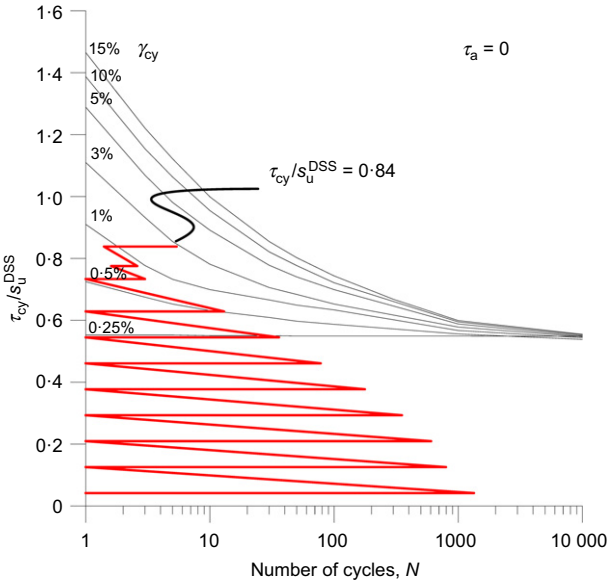

Fig. 8. The stress trajectory from cyclic accumulation of load history 1 scaled to obtain 3% cyclic shear strain in the DSS contour diagram at the end of the history including three reference cycles

table shows that the tests in each pair have the same scaling factor, such that the final strain level can be compared. Within each of the test pairs, the two tests are performed on specimens from similar depth. This reduces the uncertainty related to material variability within the test pairs.

Test pairs 2, 3, 5 and 6 consisted of an idealised and an irregular representation of the same history, as illustrated in Fig. 5. Test pair 4 was executed differently than the others as it did not compare an irregular history with an idealised history, but two idealised histories. The two histories were only different by the ordering of the groups with similar stress amplitudes. The purpose of this test pair was to compare two histories which were not influenced by the load frequency or the counting procedure. The aim of this comparison was to reveal whether the results from the other test pairs were biased by the fact that the small amplitude groups had higher load frequency, which was ignored in the idealised histories (since these had a constant load frequency throughout).

TEST RESULTS

To structure the test results from the tests shown in Table 2, the following sections are organised by first showing raw data from most of the tests and then several interpretations. Figs 9–11 show the data as measured in the lab tests. Figs 12–17 offer insight in the same test results by plotting and comparing specific parameters into different frameworks.

All ten tests in part 2 of the test programme showed a reasonable behaviour under testing. Figs 9–11 show the results from three of the test pairs. Fig. 9 shows the results from test pair 4 with load histories with low average load and idealised cyclic groups in ascending and pyramid-shaped order. The value of the reference cycles in this comparative study are clearly shown in this figure as the cyclic shear strain response reduces significantly after the peak in the pyramid-shaped load history. To evaluate whether cyclic degradation has taken place, stress cycles equal to those at the end of the history with cyclic groups in ascending order are applied (reference cycles). Fig. 10 shows the results from test pair 2 with load histories with low average load and irregular and idealised representation. Please note that both histories, also the irregular time history, generate insignificant permanent strain, thus it can be considered as a symmetric load history despite its irregular nature. Fig. 11 shows the results from test pair 5 with load histories with high average load and irregular and idealised representation. Note that the strain mainly evolves under the large stress cycles. This is observed in all test pairs, including test pair 4 with a pyramid-shaped order of the cyclic groups. The results suggest (in particular test pair 4) that for practical purposes, small cycles may be ignored in design. However, the number of small cycles can also vary for different problems and limit states being considered. Care should therefore be taken in attempts to define a threshold value for which cycles can be ignored. For the test pair 5 with irregular loading and high average level (Fig. 11), it is also clear that the larger cycles, and in particular those with high stress peaks, cause significant strain accumulation.

Reference cycle comparison

The three reference cycles applied at the end of each history are compared for a systematic assessment of the tests results. Fig. 12 shows the first of the three reference cycles in the test pairs considering the load history with negligible average load. The reference cycles from the same test pair are plotted together. The agreement is encouraging, and the deviations are considered to reflect inherent variation in the natural material. The observed cyclic strains at the end of the tests are in reasonable agreement with the predicted cyclic

Table 2. Summary of tests in part 2 of the laboratory tests programme with the purpose of assessing effect of irregular loading

Test pair	Load history	ID	Depth: m	Load history	Max. cyclic shear stress τ_{cy}/s_u^{DSS}	Average of all time stamps, τ_a/s_u^{DSS}
2	1	3A	15·75–15·95	Irregular	0·84	0·08
		3E	15·75–15·95	Idealised	0·84	0·04
3		3G	15·75–15·95	Irregular	0·88	0·09
		3F	15·75–15·95	Idealised	0·88	0·04
4		3H	15·70–15·74	Idealised (pyramid)	0·88	0·04
		3F	15·75–15·95	Idealised	0·88	0·04
5	2	4C	16·88–16·92	Irregular	0·56	0·39
		4B	16·84–16·88	Idealised	0·56	0·37
6		4E	16·93–16·95	Irregular	0·56	0·39
		4D	16·91–16·93	Idealised	0·56	0·37

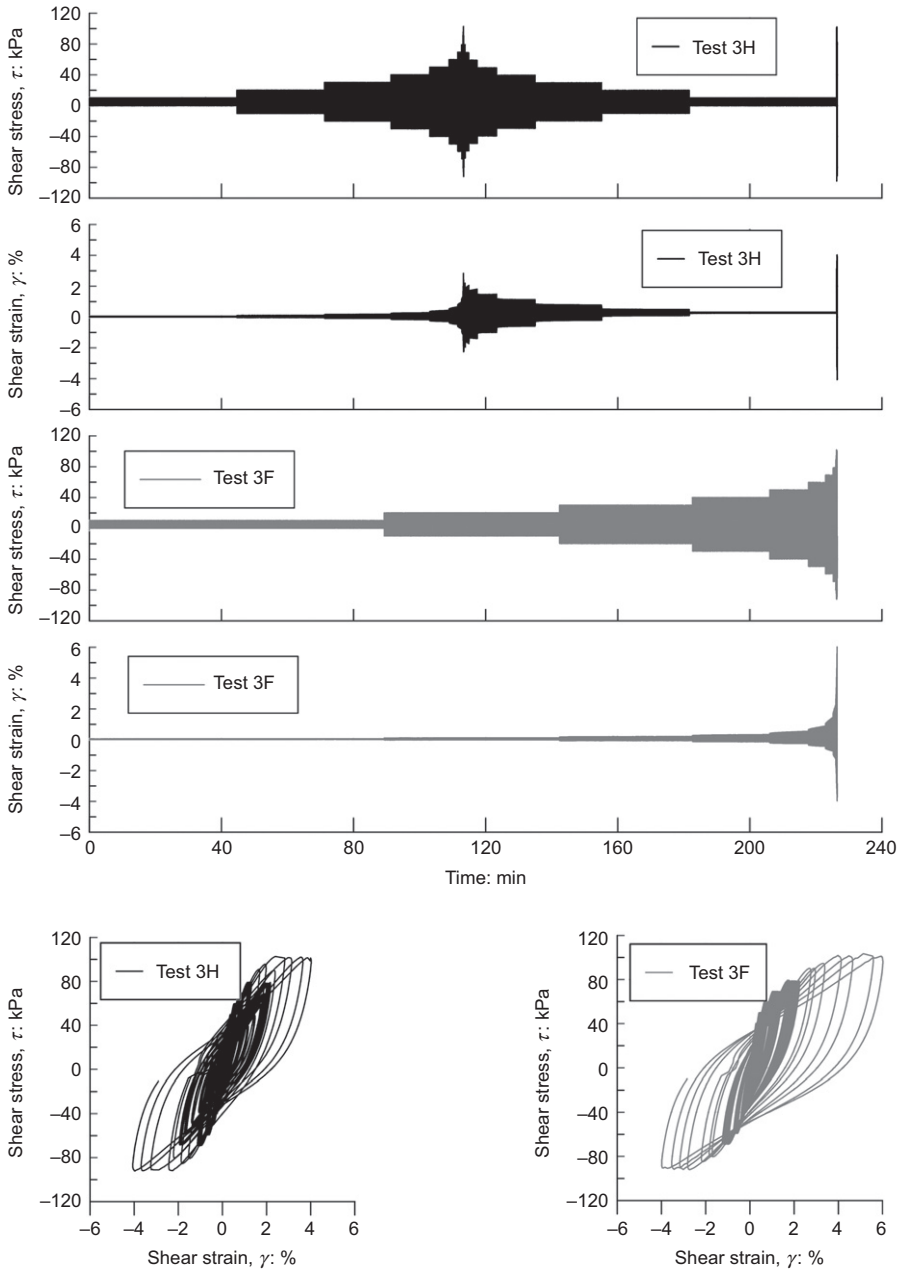

Fig. 9. Test pair 4 summary. The four figures on top show the stress history and the response as a function of time for the two tests in this test pair, which consider two idealised load histories with cyclic stress groups in pyramid shape and in ascending order. The two bottom figures show the stress–strain response for the same two tests. (Cyclic groups in pyramid-shaped order to the left and groups in ascending order to the right)

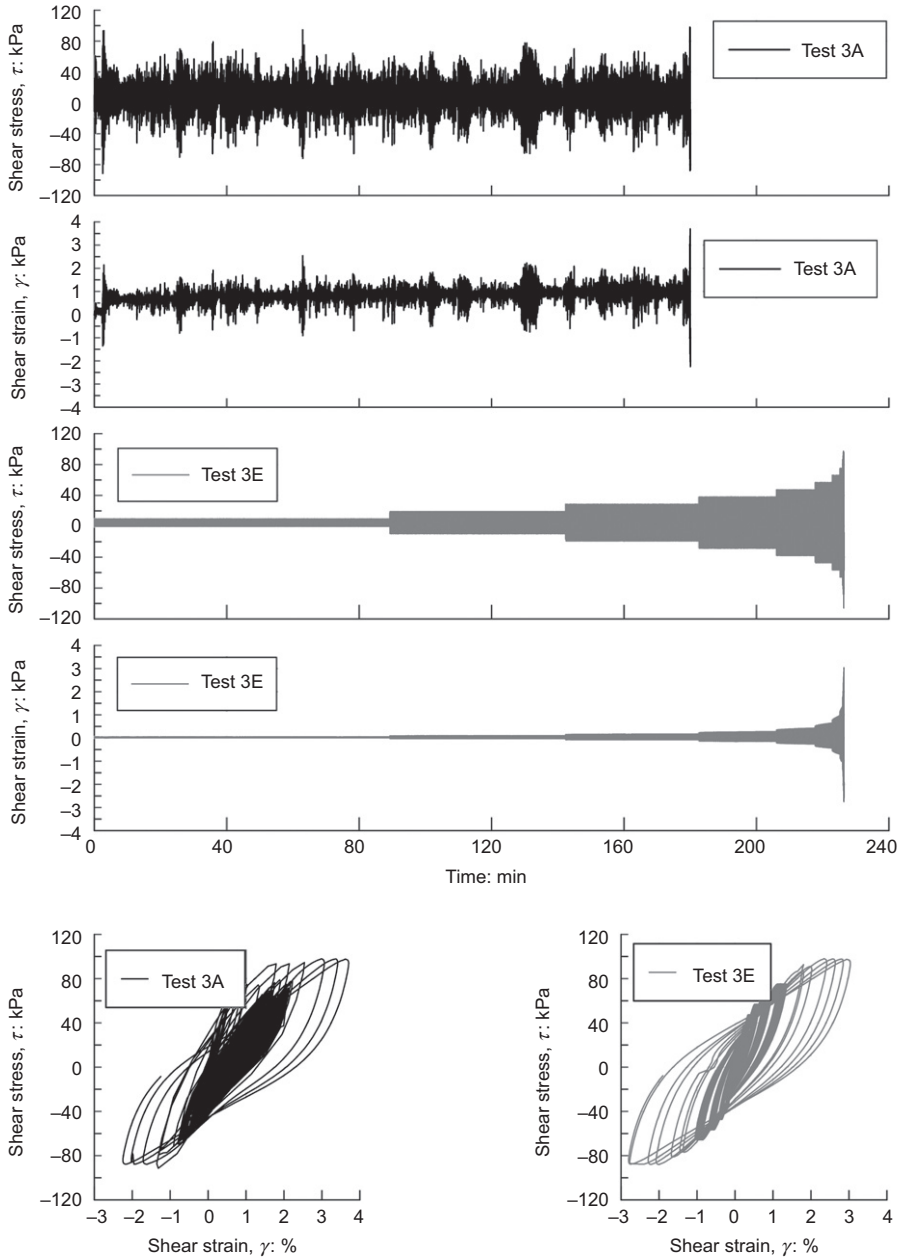

Fig. 10. Test pair 2 summary. The four figures on top show the stress history and the response as a function of time for the two tests in this test pair, which consider a history with nearly symmetric loading. The two bottom figures show the stress–strain response for the same two tests. (Irregular time history to the left and groups in ascending order to the right)

strain. This is also the conclusion from the comparison in Zografou *et al.* (2019). Fig. 13 shows the first of the three reference cycles in the test pairs considering the load history with large average load. The comparison shows that the cyclic strains in the reference cycles are very similar, while the average strain in the reference cycles following the irregular load history is somewhat larger than the average strain in the reference cycles following the idealised load history. Note that the average strain developed in the test is considerable, hence very sensitive to small variations in stress level. Fig. 14 gives an overview of the strain level in all reference tests. The cyclic strain dominates the response in the histories with low average stress, while the average strain dominates the response in the histories with low cyclic stress. Please note that even if only the first out of the three reference cycles is included in these figures, similar relative differences are given.

Comparison of equivalent strength

The tests, performed as they are, give no direct information about the cyclic shear strength at the end of the cyclic test history. However, by utilising the contour diagram, N_{eq} can be determined for each test based on the strain and stress level in the reference cycles. The cyclic shear strength at this N_{eq} can then be used for comparison. (The cyclic shear strength is defined at the 15% cyclic shear strain contour.) Fig. 15 illustrates this procedure for test pair 2. The crosses in the figure give the degradation or state at the end of history in tests 3A and 3E. The vertical arrows relate this degradation to the equivalent cyclic shear strength defined by the failure line for this N_{eq}. In addition to the relative difference between the tests, the procedure also gives a comparison between the test results and the cyclic accumulation procedure. The strain level and N_{eq} were predicted prior to the testing to find the appropriate stress level in the tests. The strain level predicted

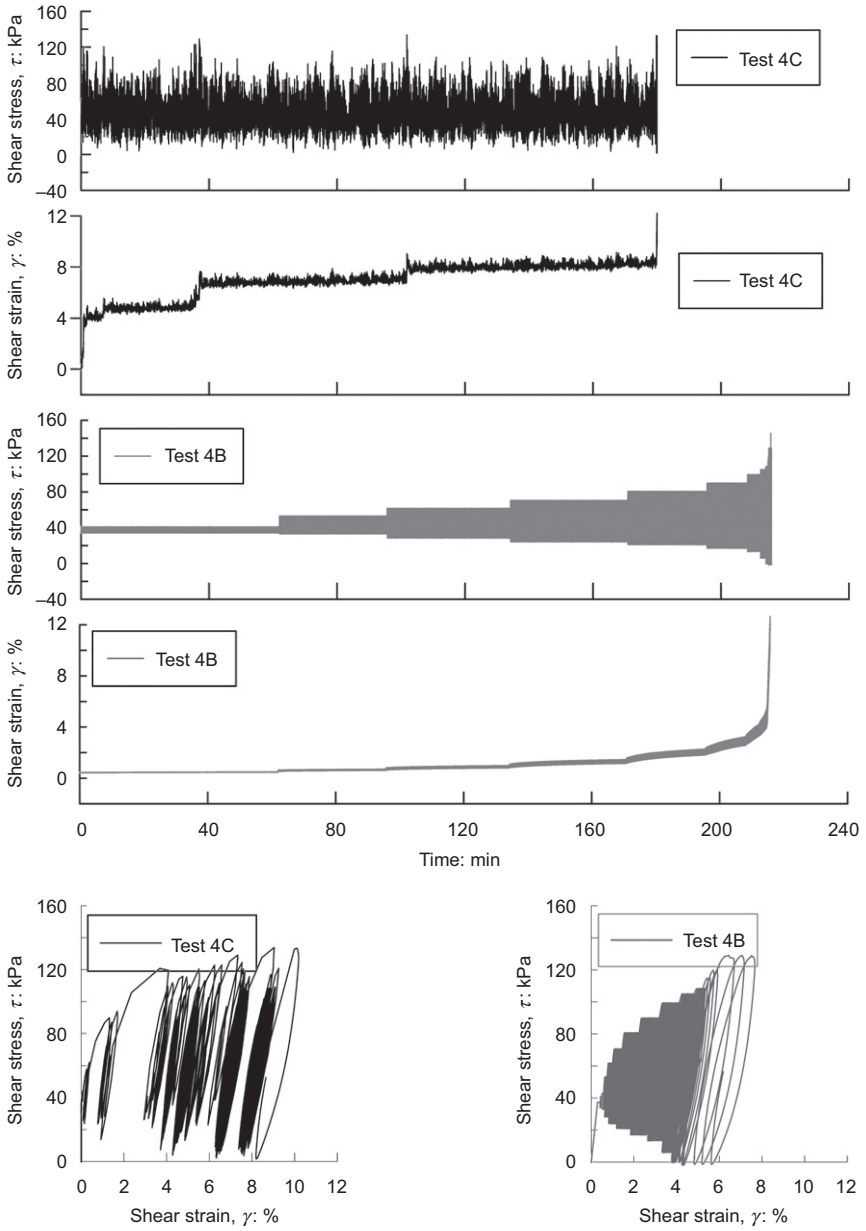

Fig. 11. Test pair 5 summary. The four figures on top show the stress history and the response as a function of time for the two tests in this test pair, which consider a history with high average load. The two bottom figures show the stress–strain response for the same two tests. (Irregular time history to the left and groups in ascending order to the right)

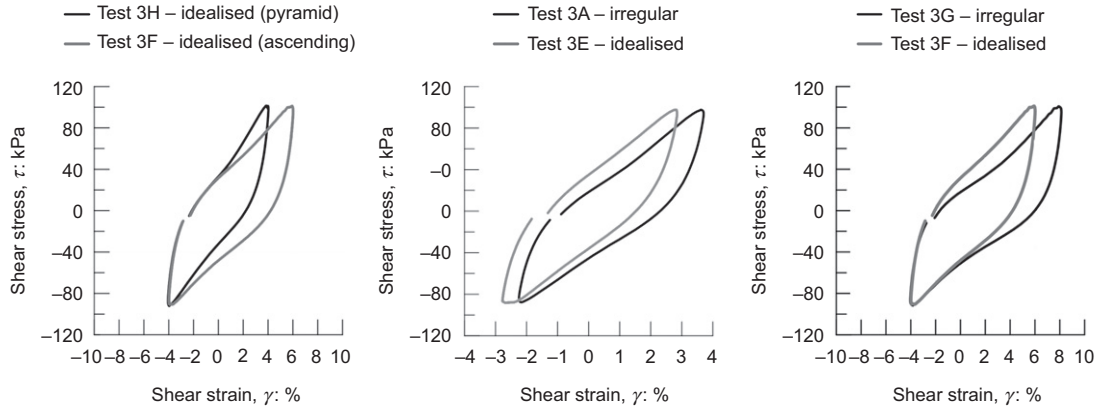

Fig. 12. Comparison of reference cycles in test pairs 2, 3 and 4

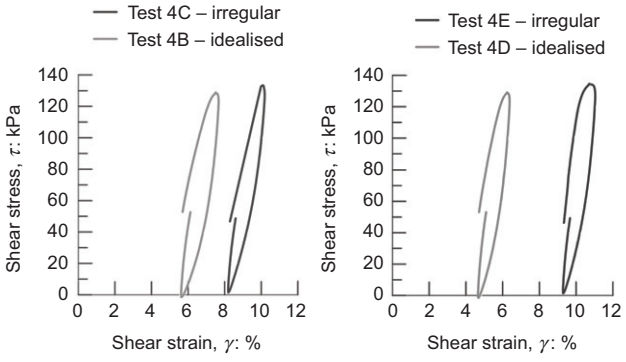

Fig. 13. Comparison of reference cycles in test pairs 5 and 6

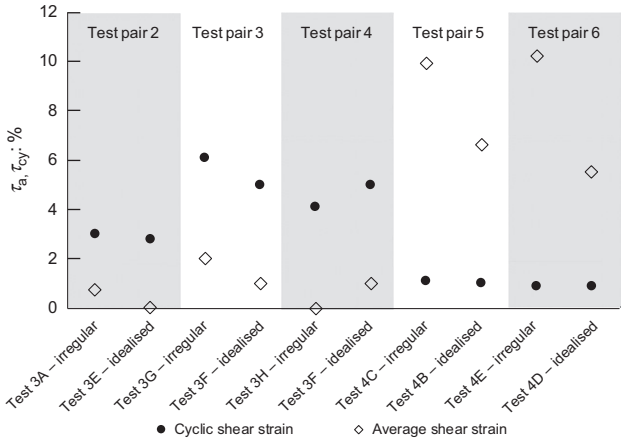

Fig. 14. Cyclic and average shear strength in all tests

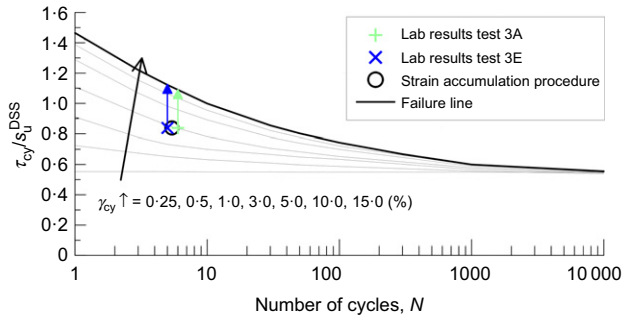

Fig. 15. Interpretation of laboratory results by contour diagram, focusing on cyclic strain

for test pair 2 is indicated in Fig. 15 and can be compared with the test results. The strain accumulation was performed in a 2D cross-section which reflects a cyclic-to-average stress ratio of the largest load. The same comparison as shown in Fig. 15 was performed for all test pairs. For test pairs 2, 3 and 4, the cyclic shear strain, γ_{cy}, was used as the state or memory parameter in the accumulation procedure. For test pairs 5 and 6, the average shear strain, γ_a, was used as the state or memory parameter in the accumulation procedure. Table 3 summarises the interpreted cyclic shear strength determined by this procedure for all the test results. The cyclic shear strength is given by the relevant component $\tau_{cy,f}$ for test pairs 2, 3 and 4 and $\tau_{a,f}$ for test pairs 5 and 6. The agreement between the irregular and idealised tests, and the agreement between the predictions and the tests, are acceptable and do not exceed 10% for any of the test pairs.

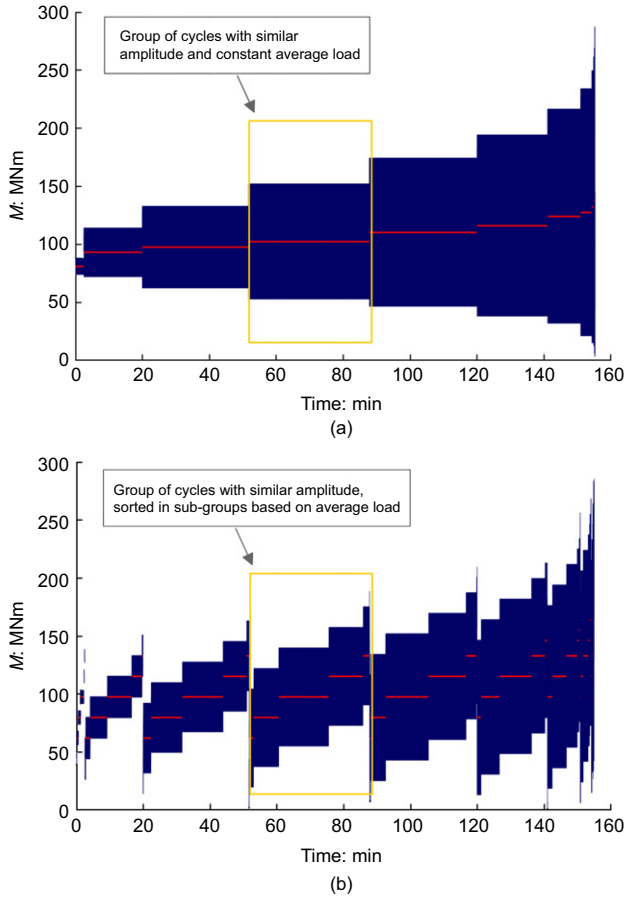

Fig. 16. Illustration of two representations of the average load

Discussion on the difference in average strain

The test results from test pairs 4 and 5 (large average load) show that the accumulation of average strain is more sensitive to the representation of the history than the magnitude of the cyclic strain. This may appear to disagree with the finding from Zografou *et al.* (2019), which finds the strain accumulation procedure to overestimate the predicted strain through the assumption that the amplitude should be arranged in ascending order. However, this paper is rather complementary, as it considers the strain generated under 'true' irregular time histories. The higher strain developed under non-symmetric irregular loading in this paper is caused by the transformation of the original history, not by the ordering of cyclic groups as studied by Zografou *et al.* (2019). A closer look at Fig. 16 shows one possible explanation for the deviation in test pairs 4 and 5. When the Rainflow counting method is used in the translation of the irregular histories, the average load of a group of cycles is commonly calculated by averaging all average values of the cycles in the group. The idealised history translated by this procedure is shown in Fig. 16(a). A more refined representation is shown in Fig. 16(b) where the history is sorted not only by the cyclic amplitude but also by the average load.

By comparing the two histories, it becomes clear that the history in Fig. 16(a) is missing some of the high average or peak loads from the irregular history. This may reduce the accumulation of average (and permanent) strain since the cycles with high peak loads particularly influence the development of average strain. Even if this observation is reasonable based on existing knowledge, it has been somewhat neglected in design, where histories typically are translated by averaging all cycles within an amplitude group (Fig. 16(a)). This may lead to an under-prediction of

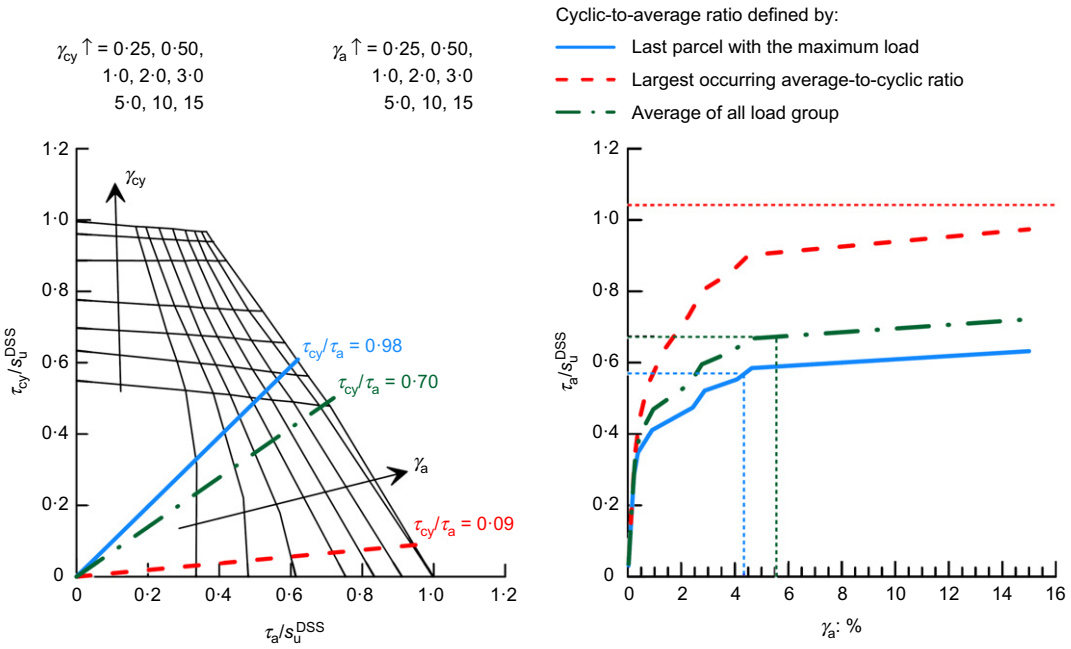

Fig. 17. Illustration of extracted strain–strain curves based on different cyclic-to-average ratios

Table 3. Predicted and interpreted cyclic shear strength through N_{eq}

Test pair with negligible average load				
Test pair	Load history	ID	N_{eq}	Interpreted cyclic shear strength, $\tau_{cy,f}/s_u^{DSS}$
Test pair 2	Load history 1	3A	5·0	1·09
		3E	4·5	1·13
		Predicted	5·4	1·11
Test pair 3		3F	11·0	0·99
		3G	13·0	0·97
		Predicted	6·8	1·07
Test pair 4		3H	7·0	1·07
		3F	11·0	0·99
		Predicted	6·8	1·08

Test pair with large average load				
Test pair	Load history	ID	N_{eq}	Interpreted average shear strength $\tau_{a,f}/s_u^{DSS}$
Test pair 5	Load history 2	4C	22·0	0·59
		4B	13·0	0·61
		Predicted	7·8	0·63
Test pair 6		4E	23·0	0·58
		4D	10·0	0·62
		Predicted	7·8	0·63

average and permanent strain. It should not, however, be forgotten that the difference in cyclic shear strength, as given in Table 3, is minor. This is because strain contours are closely spaced near the failure line, and the prediction of strain close to failure becomes more difficult than prediction of the cyclic shear strength.

DESIGN RECOMMENDATIONS FOR HISTORIES WITH LARGE AVERAGE LOADS

An average shear strain of approximately 6% was predicted for test pairs 5 and 6. The final average strain observed in the tests with idealised load histories deviated no more than 15% from the predictions. This agreement is sufficient from a design perspective. However, compared to the final average strain in the test with the irregular load history, the predictions under-estimate the accumulated average strain by approximately 40%. This indicates that some information is lost in the translation to an idealised history. When strain accumulation is applied in design, it is common to assume a constant cyclic-to-average stress ratio for the entire history. The accumulation can then be performed by extracting the relevant 2D cross-section from the 3D contour diagram. This is the approach taken in the current paper. However, a constant ratio may fail to represent the whole history, since the cyclic-to-average stress ratio varies throughout the irregular history. A possible improvement to the method would be to include the variable average stress in the

accumulation procedure. That would mean that the strain accumulation must be performed in a full 3D diagram. There is, however, no straightforward way to update the memory parameter (e.g. γ_a) when the average stress reduces. In addition, performing strain accumulation in a full 3D space becomes extremely complex and the procedure loses some of its attractive simplicity.

An alternative is to keep the strain accumulation procedure as is, but address the uncertainty in the cyclic-to-average stress ratio by considering a range of this ratio that captures this uncertainty. The strain accumulation for test pairs 5 and 6 was performed in cross-section of the contour diagram where $\tau_{cy}/\tau_a = 0{\cdot}56/0{\cdot}57 = 0{\cdot}98$. This corresponds to the ratio of the final applied amplitude group including the reference cycles and reflects the most common way to define the governing cyclic-to-average load ratio. However, to address variation in cyclic-to-average load throughout the history, the cyclic accumulation procedure was also carried out for two different cyclic-to-average load ratios. Thus, three 2D cross-sections (τ_{cy}–N) with different cyclic-to-average ratios were extracted from the full 3D diagram

(*a*) cyclic-to-average load ratio corresponding to the final (and largest) amplitude group, $\tau_{cy}/\tau_a = 0{\cdot}98$
(*b*) average of all cyclic-to-average load ratios, $\tau_{cy}/\tau_a = 0{\cdot}70$
(*c*) the minimum cyclic-to-average load ratio of all cyclic groups, $\tau_{cy}/\tau_a = 0{\cdot}09$.

The accumulation method was performed with the same history and all three 2D diagrams (τ_{cy}–N), giving three average stress plotted against average strain curves up to failure ($\gamma_a = 15\%$). Each ratio gave a number of equivalent cycles, N_{eq}, close to 10. Fig. 17(a) shows the 2D cross-section of the contour diagram at $N = 10$ representative for all the three ratios. Fig. 17(b) shows the stress–strain curves obtained from the strain accumulation. The average strain at the end of the history can be estimated by combining the final average stress and the corresponding curve in Fig. 17(b). Note that the final average stress must reflect the assumed cyclic-to-average ratio of the curve. Thus, three horizontal lines are shown in Fig. 17(b) indicating the three relevant average stress levels. In this paper, the average stress levels are referred to as the updated average stress $(\tau_{a,u})$. This average stress is determined by keeping the peak load constant ($\tau_{cy} + \tau_a =$ constant) and includes the cyclic-to-average stress ratio under consideration $(\tau_{cy}/\tau_a)_u$. The updated average stress can be found by the simple formula

$$\tau_{a,u} = \frac{\tau_{cy} + \tau_a}{1 + (\tau_{cy}/\tau_a)_u} \quad (1)$$

Figure 17 shows that for a low cyclic-to-average stress ratio, the average stress–average strain curve is stiffer and has a higher average shear strength. However, the ratio considered gives a consistently higher average shear stress at peak ($(\tau_{cy}/\tau_a)_u = 1{\cdot}04$) and overestimates the average strain by predicting failure. The two other ratios lead to an average strain, γ_a, prediction of 4·3% and 5·6% found by the intersection of the vertical lines with the horizontal axis. This compares with approximately $\gamma_a = 6\%$ in the tests with idealised load histories and approximately $\gamma_a = 10\%$ in the tests with irregular load histories. This exercise highlights the importance of the sensitivity assumed when specifying the cyclic-to-average load ratio. When similar load histories are driving the design, the authors recommend applying a high and a low estimate of the cyclic-to-average load ratio. These considerations are also relevant for problems where the cyclic load dominates but significant average strain can occur with relatively small average load (i.e. lateral spreading in liquefaction). The contour diagrams for the relevant material give an indication of when this can happen as the average contours are moving closer to the vertical axis when the cyclic stress increase. Based on the 2D cross-section in Fig. 17 (left), average failure may occur at only 40% of the monotonic capacity. The dominating strain (cyclic or average) should also affect the choice of memory parameter used in the accumulation procedure, as investigated by Andersen *et al*. (1992).

CONCLUSIONS

The cyclic DSS tests presented here have given new insight regarding the response of clay subjected to irregular cycling loading. Overall, the results suggest that the translation of irregular time histories to idealised histories by the Rainflow counting method is a reasonable engineering approach to account for the effect of cyclic loading in design. The uncertainty introduced by the translation appears to be limited. However, these results are based on one clay and a limited amount of possible loading conditions, and more testing should be performed to extend the empirical basis. The laboratory test programme compared the soil response in reference cycles applied after the idealised and irregular cyclic histories and the comparison showed that

(*a*) the cyclic strain in the reference cycles applied after the test history were very similar, suggesting that the degradation was the same at the end of the history
(*b*) the test subjected to irregular loading with high average load accumulated somewhat more average strain than the tests subjected to the idealised loading
(*c*) the interpreted equivalent cyclic shear strength at the end of the cyclic tests was compared with the cyclic shear strength predicted by the strain accumulation procedure. The agreement was satisfactory with a maximum deviation of 10%.

The comparison revealed that the development of average strain is most sensitive to the representation of the loading. This is especially predominant for load histories with a large average load. The reason for this discrepancy is likely not to be explained by the order of load cycles itself. A more reasonable explanation is that the Rainflow counting procedure erases the load cycles with the highest average load due to averaging of the average load within the cyclic group. This will remove peak stresses from within the idealised history.

The sensitivity in the prediction of average and permanent strain developed under cyclic loading with high average load should influence design practice if permanent strains are driving the design. The authors recommend examining the sensitivity of the assumed cyclic-to-average load ratio in such cases, and a procedure is proposed in this paper.

Similar studies available in the public domain have focused mainly on the reliability of the accumulation method to idealised histories with cyclic groups in various orders. This study adds complementary knowledge to the existing studies and together they suggest that the commonly used design assumptions consisting of translation of irregular time histories and then ordering of cyclic groups by ascending amplitude is reasonable and has sufficient accuracy.

ACKNOWLEDGEMENTS

The authors wish to gratefully acknowledge the financial support by the Norwegian Research Council and the industrial partners Equinor, Innogy, EDF and Multiconsult

through the project 'Wave loads and soil support for extra large monopiles' (WAS-XL), grant no. 268182. In addition, the authors would like to thank Karin Norén-Cosgriff, Knut H. Andersen, Tariq Abdu and Steven Bayton for their contribution.

NOTATION

H_S	significant wave height
M	overturing moment applied to the monopile at mudline
N	number of cycles
N_{eq}	equivalent number of cycles
N_f	number of cycles to failure
s_u^{DSS}	undrained direct shear strain (DSS) shear strength
T_p	spectral peak period
u_a	average pore pressure
u_{cy}	cyclic pore pressure
γ_a	average shear strain
$\gamma_{a,f}$	average shear strain at failure
γ_{cy}	cyclic shear strain
$\gamma_{cy,f}$	cyclic shear strain at failure
γ'	effective unit weight
σ'_{v0}	axial consolidation stress
τ_a	average shear stress
$\tau_{a,u}$	updated average stress
τ_{cy}	cyclic shear stress

REFERENCES

Achmus, M., Kuo, Y. S. & Abdel-Rahman, K. (2009). Behavior of monopile foundations under cyclic lateral load. *Comput. Geotech.* **36**, No. 5, 725–735.

Andersen, K. H. (1976). Behaviour of clay subjected to undrained cyclic loading. In *Proceedings of the international conference on the behaviour of offshore structures (BOSS 76)*, vol. 1, pp. 392–403. Trondheim, Norway: Norwegian Institute of Technology.

Andersen, K. (2015). Cyclic soil parameters for offshore foundation design. In *Frontiers in offshore geotechnics III* (ed. V. Meyer), vol. 1, pp. 5–82. Boca Raton, FL, USA: CRC Press.

Andersen, K. H., Dyvik, R., Yoshiaki, Y. & Skomedal, E. (1992). Clay behaviour under irregular cyclic loading. In *Proceedings of the 6th international conference on the behaviour of offshore structures (BOSS 92)* (eds M. H. Patel and R. Gibbins), vol. 2, pp. 937–950. London, UK: BPP Technical Services.

Bjerrum, L. & Landva, A. (1966). Direct simple-shear tests on a Norwegian quick clay. *Géotechnique* **16**, No. 1, 1–20, https://doi.org/10.1680/geot.1966.16.1.1.

IEC (International Electrotechnical Commission) (2009). IEC 61400-3: 2009: Wind turbines – Part 3: Design requirements for offshore wind turbines. Geneva, Switzerland: International Electrotechnical Commission.

Ishihara, K., Tatasuoka, F. & Yasuada, S. (1975). Undrained deformation and liquefaction of sand under cyclic stresses. *Soils Found.* **15**, No. 1, 29–44.

Lade, P. V. (2016). *Triaxial testing of soils*. New York, NY, USA: John Wiley & Sons.

Leblanc, C., Byrne, B. W. & Houlsby, G. T. (2009). Response of stiff piles in sand to long-term cyclic lateral loading. *Géotechnique* **60**, No. 2, 79–90, https://doi.org/10.1680/geot.7.00196.

Liu, H. Y., Abell, J. A., Diambra, A. & Pisanò, F. (2019). Modelling the cyclic ratcheting of sands through memory-enhanced bounding surface plasticity. *Géotechnique* **69**, No. 9, 783–800, https://doi.org/10.1680/jgeot.17.P.307.

Matsuishi, M. & Endo, T. (1968). *Fatigue of metals subjected to varying stress*, paper presented to the Japan Society of Mechanical Engineers. Fukuoka, Japan: Japan Society of Mechanical Engineers.

Mróz, Z., Norris, V. A. & Zienkiewicz, O. C. (1981). An anisotropic, critical state model for soils subject to cyclic loading. *Géotechnique* **31**, No. 4, 451–469, https://doi.org/10.1680/geot.1981.31.4.451.

Niemunis, A., Wichtmann, T. & Triantafyllidis, T. (2005). A high-cycle accumulation model for sand. *Comput. Geotech.* **32**, No. 4, 245–263.

Norén-Cosgriff, K., Jostad, H. P. & Madshus, C. (2015). Idealized load composition for determination of cyclic undrained degradation of soils. In *Frontiers in offshore geotechnics III* (ed. V. Meyer), vol. 2, pp. 1097–1102. Boca Raton, FL, USA: CRC Press.

Seed, H. B. (1968). Landslides during earthquakes due to liquefaction. *J. Soil Mech. Found. Div.* **94**, No. SM5, 1055–1122.

Seed, H. B. & Lee, K. L. (1966). Liquefaction of saturated sands during cyclic loading. *J. Soil Mech. Found. Div.* **92**, No. 6, 105–134.

Skau, K. S. & Jostad, H. P. (2014). Application of the NGI-procedure for design of bucket foundations for offshore wind turbines. In *Proceedings of the twenty-fourth (2014) international ocean and polar engineering conference (ISOPE)* (eds J. S. Chung, F. Vorpahl, S.-W. Hong, S. Y. Hong, T. Kokkinis and A. M. Wang), pp. 189–198. Cupertino, CA, USA: International Society of Offshore and Polar Engineers.

Taiebat, M. & Dafalias, Y. F. (2008). SANISAND: simple anisotropic sand plasticity model. *Int. J. Numer. Analyt. Methods Geomech.* **32**, No. 8, 915–948.

Wichtmann, T. (2005). *Explicit accumulation model for non-cohesive soils under cyclic loading*. PhD thesis, Ruhr-University Bochum, Bochum, Germany.

Wichtmann, T., Niemunis, A. & Triantafyllidis, T. (2009). Validation and calibration of a high-cycle accumulation model based on cyclic triaxial tests on eight sands. *Soils Found.* **49**, No. 5, 711–728.

Zografou, D., Gourvenec, S. & O'Loughlin, C. D. (2019). Response of normally consolidated kaolin clay under irregular cyclic loading and comparison with predictions from the accumulation procedure. *Géotechnique* **69**, No. 2, 106–121, https://doi.org/10.1680/jgeot.16.P.340.